ViSkin: Physics-based Simulation of Virtual Skin on Personalized Avatars

Davide Corigliano, Juan Sebastian Montes Maestre,
Ronan Hinchet, Stelian Coros, Bernhard Thomaszewski
ETH Zürich
Switzerland
{dcorigliano, jmontes, rhinchet, scoros, bthomasz}@ethz.ch

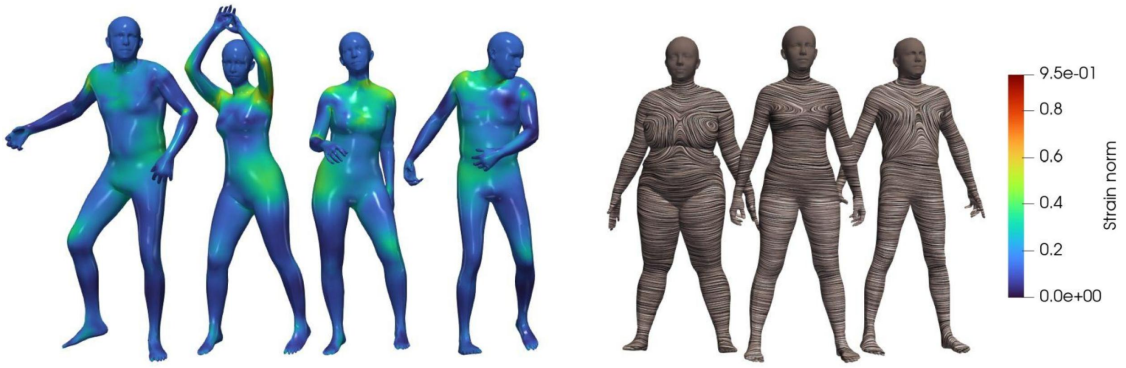

Figure 1. ViSkin adds skin simulation capabilities to personalized avatars. Based on a novel, biomechanically principled material model, our method captures the salient characteristics of human skin, including nonlinear stretching resistance, anisotropic stiffness, spatially varying sliding properties, and direction-dependent pre-stretch according to *Langer lines* (right). As illustrated on the left, ViSkin produces smooth, physically plausible skin deformations for arbitrary body shapes and poses.

Abstract

We introduce ViSkin, a biomechanically principled approach to simulate skin mechanics on personalized avatars. Our model captures the salient characteristics of human skin, i.e., nonlinear stretching properties, anisotropic stiffness, direction-dependent pre-stretch, and heterogeneous sliding behavior. In particular, we introduce a novel representation of Langer lines, which describe the distribution of principal material directions across the human body. We further propose an optimization-based approach for inferring spatially-varying pre-stretch from motion capture data. We implement our new model using a computationally efficient intrinsic representation that simulates skin as a two-dimensional Lagrangian mesh embedded in the three-dimensional body surface. We demonstrate our method on a diverse set of body models, shapes, and poses and compare to experimentally-obtained skin motion data. Our results indicate that our method produces smoother and more plausible skin deformations than a baseline method and shows good accuracy compared to real-world data.

1. Introduction

The advent of personalized digital body models such as SMPL [27] and STAR [36] points towards a future in which the real and virtual worlds are seamlessly integrated. Progress in these models leads to lifelike digital humans, capturing nuances in appearance, motion, and expressions. As they become increasingly accessible, new possibilities emerge in entertainment and applications abound in apparel, health, and medical sectors. Beyond mere appearance, recent research has started to augment digital humans with personalized anatomical structures such as bones [16], organs [13, 42], and muscles [3, 20]. These biomechanical models open up new opportunities for personalized diagnostics and therapeutics, engineering safety, and rehabilitation. However, to fully unlock the potential of these advancements, we must first be able to predict and simulate the complex functions of these biomechanical models. Initial forays in this direction have already been made to emulate, e.g., fat and muscle deformations during motion. Although these extensions may increase the perceived realism of digital humans, undifferentiated treatment of soft tissue neglects the complex mechanics of hu-

man skin and their importance in applications. Given its unique multi-layer composition intertwined with collagen fibers, the complexities of modeling human skin with its nonlinear and anisotropic behaviors are profound. Nevertheless, the ability to simulate personalized skin mechanics would open up new opportunities in the design of made-to-measure sportswear, patient-specific orthoses, and robotic assistive devices such as exoskeletons. Computational modeling of skin is an active area of research, but, to the best of our knowledge, no model exists that would generalize to body-scale simulation on personalized digital avatars.

In this paper, we propose ViSkin—a simple yet biomechanically principled approach to simulate skin mechanics on digital body models. Our contributions are as follows:

- **Efficient and Physically-Principled Model**: We present a model that efficiently captures the complex mechanics of human skin on digital body models, including both stretching and sliding. In particular, our approach incorporates a sophisticated material model that faithfully represents the non-linear, anisotropic, and pre-stretched nature of human skin.
- **Representation of Langer Lines**: We introduce a novel representation of Langer lines as on-surface vector fields. These fields define the local axes for the tissue anisotropy.
- **Representation of Spatially Varying Adhesion**: We present a model for skin ligaments that accounts for the localized attachment of skin to the underlying tissue structure.
- **Optimization-based Pre-Stretch Computation**: We propose an optimization-based method for computing ideal per-element pre-stretch tensors to minimize elastic energy across a large set of real-world body motion data.

We demonstrate ViSkin on a diverse set of body shapes and motions taken from real-world capture data. We further calibrate and evaluate our skin model through experiments.

2. Related work

Digital Humans. Fueled by technological innovation in static and mobile capturing devices, digital humans have seen tremendous progress in the past two decades [2, 5, 6]. Today, personalized body models enable the rapid creation of high-quality digital twins for arbitrary individuals [4, 27, 36]. In addition to visual appearance and pose, research has started to augment personalized body models with anatomical structures such as bones [16, 17], organs [13, 42], and muscles [3, 20]. In this work, we aim to further expand the envelope of digital humans with a tailored solution for simulating skin mechanics on personalized body models.

Flesh Simulation. Simulating the outer layer of a character involves two main components: the *skin*, i.e., the comparatively thin layer covering the human body, and the *flesh*, i.e., the soft tissue below the skin. Soft tissue simulations typically focus on fat and muscle tissues—often in a homogenized way—without explicit consideration of skin mechanics [29, 31, 45, 47, 48]. A recent line of work has explored the incorporation of soft tissue deformations in digital body models, using combinations of data-driven and simulation-based techniques [18, 38–41]. We note that simulating skin and soft tissue are two different and complementary problems. In particular, a homogenized treatment of soft tissue with volumetric finite elements cannot account for sliding and other nonlinear effects observed in human skin. To the best of our knowledge, our work is the first to consider body-scale skin simulation on personalized avatar models.

Skin Simulation. Simulating skin deformation is a problem that has been intensively investigated in the computer graphics literature. Early approaches were mostly based on mass-spring systems [1, 33, 49, 53], whereas more recent work has turned to advanced finite element modeling [26, 54]. Skin exhibits strongly anisotropic properties, which must be taken into account for accurate modeling [19]. Biomechanical models are typically based on energy density functions whose parameters are fitted to best approximate the mechanical behavior of real human or animal skin patches subject to tensile tests [10, 23, 24]. Anisotropy is often incorporated by augmenting an isotropic base material with stiffer (collagen) fibers [12, 52]. While existing biomechanical models are remarkably complex, they focus on the tensile behavior of simple isolated patches. Our work, in contrast, aims to simulate skin deformations across the entire human body, taking into account skin sliding as well as spatially-varying adhesion, fibers and pre-stretch directions.

Coupling Tissue and Body. Skin is coupled with the underlying muscles and bones through a complex stack of contacting tissue layers intertwined with skin tendons and ligaments. Due to this complex composition, explicitly modeling skin layers and handling contact between them is extremely challenging. A simplification proposed by Li et al. [26] is to resort to an Eulerian-on-Lagrangian representation [9, 46, 51], in which the skin is modeled with Eulerian (texture-like) coordinates relative to a Lagrangian body mesh. This Eulerian-on-Langrangian discretization allows skin to freely slide on the body mesh while avoiding contact handling altogether. However, this approach requires a parameterization of the body mesh using an atlas of quasi-isometric patches of skin. In the context of skintight clothing design, Montes et al. [32] explored a Lagrangian-on-Lagrangian approach in which a two-dimensional Lagrangian mesh, representing the clothing, is embedded in a three-dimensional body mesh. Another alternative is

to represent clothing as a three-dimensional mesh and to handle contact between cloth and body explicitly [50]. We opt for a Lagrangian-on-Lagrangian skin representation which, compared to the work of Li et al. [26], avoids the complexity of creating a skin atlas.

Mechanical Properties of Skin. The material constants for biomechanical skin models are typically determined using tensile tests on small patches of skin [10, 12, 23–25]. By analyzing patches distributed across the body, Ni Annaidh et al. [35] experimentally confirmed the existence of large variations in principal directions.

Our method builds on a biomechanical material model of human skin. To determine principal directions across the body, we leverage the concept of Langer lines, i.e., lines of principal skin tension that were discovered and experimentally determined more than 150 years ago [21, 22]. We translate these experimental maps into detailed whole-body vector fields that serve as the basis for both material anisotropy in stiffness and pre-stretch. To the best of our knowledge, this is the first computational model of human skin to include Langer lines.

3. Anatomy & Physiology of Human Skin

Before describing our bio-inspired computational model of skin, we provide a brief overview of the structures and mechanical functions of human skin.

3.1. Skin Anatomy

Human skin is a complex organ whose structure can be decomposed into three main layers [37]. As shown in Figure 2, the outermost layer is the *epidermis*, which functions as an interface with the external world. The *dermis* contains high densities of collagen and elastin fibers, playing a central role for the mechanical properties of the skin. Finally, the *hypodermis* is a layer of adipose tissue that minimizes friction with the underlying structures, thus allowing skin to slide. The adipose tissue is crossed by skin ligaments [34, 44] that attach the skin to the underlying structures. These ligaments restrain the skin from sliding arbitrarily, with the range of freedom depending on the ligament lengths and density [7].

3.2. Langer Lines, Pre-Stretch, and Ligaments

Human skin is stretched across the body in anisotropic ways, with the direction of maximum stretch following tension lines [8, 22]. These lines, which are also called Langer lines, cause incisions to open by different amounts depending on their orientation and location on the body. The knowledge of these directions is therefore crucial for surgeons, as Langer lines influence the cicatrization of wounds. Langer lines have been shown to correlate with directions of both maximum pre-stretch and stiffness [35].

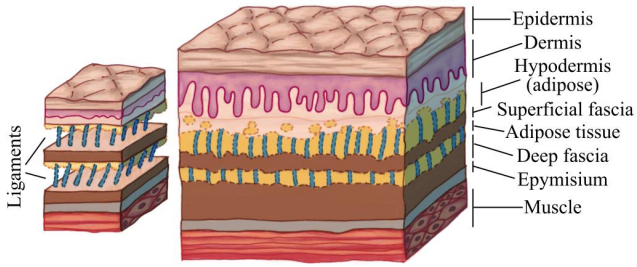

Figure 2. Skin structure. On the right, skin classification in layers. On the left, skin relations with neighboring structures. Skin ligaments crossing the adipose tissue are shown in blue on the left.

Pre-stretch, anisotropic stiffness, and ligaments are distinct but coupled mechanisms that govern the skin's complex behavior. Collagen fibers induce pre-stretch and stiffening along the Langer lines, thus determining the skin's response to deformation. Imposing limits on skin sliding, ligaments induce a complementary effect that does not directly influence the elastic properties of the tissue. We observe that a stiffer skin material alone cannot produce the bi-phasic anchoring effect of ligaments.

We argue that a biomechanically meaningful model for body-scale skin simulation must be able to capture the nonlinear and anisotropic stiffness of skin as well as spatially-varying pre-stretch and sliding limits. As we explain next, our model implements each of these mechanisms in a physically principled way.

4. Computational Modeling of Human Skin

This section presents our computational method for large-scale skin simulation on personalized digital body models. We start with our discrete representation for skin (Sec. 4.1) before proceeding to material modeling (Sec. 4.2). We then describe extensions to incorporate pre-stretch and how to determine optimal values from data (Sec. 4.3). Finally, we introduce a mechanism to implement the sliding-limiting effects of skin ligaments (Sec. 4.4).

4.1. Discrete Representation

We discretize skin using a linear finite element approach based on constant-strain triangles. To avoid contact handling between skin and body, we use a Lagrangian-on-Lagrangian representation (similar to Montes et al. [32]) and embed skin directly in the body mesh. Other than body-skin collisions, this approach also avoids self-contact handling, as tissue motion is constrained to be a pure sliding. We represent a given skin node through barycentric coordinates of its corresponding body triangle $\mathbf{s}_i = (u_i, v_i, t_j) \in R^{[0,1]^2 \times N}$, and we enable smooth skin sliding by modeling the body mesh as a subdivision surface—see Montes et al. [32] for details. To compute the subdivision surface, we use

the freely available implementation from the OpenSubdiv library. With this setup, simulating skin amounts to finding the deformed state $\mathcal{S}$ given the current body configuration $\mathcal{B}$ and the rest state of the skin $\bar{\mathcal{S}}$. Whenever the body moves or deforms, the skin must remain in equilibrium, i.e.,

$$\hat{\mathbf{S}} = \text{argmin}_{\mathbf{S}}\ E(\mathcal{F}(\mathbf{S}), \mathcal{F}(\tilde{\mathbf{S}})) \quad \text{s.t. } \mathbf{f}(\mathcal{F}(\mathbf{S}), \mathcal{F}(\bar{\mathbf{S}})) = 0 \tag{1}$$

where $\hat{\mathbf{S}}$ and $\bar{\mathbf{S}}$ are barycentric coordinates of skin vertices in the deformed and undeformed state, respectively. $\mathbf{f} = -\nabla_{\mathbf{S}} E(\mathbf{S}, \bar{\mathbf{S}})$ is the vector of elastic per-vertex forces, E is the elastic energy of the skin, and $\mathcal{F}$ evaluates the subdivision surface to determine the 3D world-space positions of the skin nodes given the corresponding barycentric coordinates. Next, we describe how we model the elastic potential of the skin.

4.2. Material Modeling

Simple approaches often approximate skin behavior using a polynomial elastic model such as the Mooney-Rivlin family. However, this class of materials cannot adequately model stiffening, which is an effect observed in many types of biological tissue for large deformations [10]. Besides stiffening, another important nonlinearity is due to the fact that skin wrinkles under compression, which corresponds to a substantial reduction in stiffness. To account for both these effects, we build our model on the stabilized Fung energy proposed by Smith et al. [43],

$$W_{Fung} = \underbrace{\frac{\mu}{2}(I_1 - 2)}_{\text{Polynomial}} + \underbrace{\frac{\lambda}{2}(J-k)^2}_{\text{Area preservation}} + \underbrace{\frac{\alpha}{2}(e^{\frac{\beta}{2}(I_1-2)} - 1)}_{\text{Exponential stiffening}} \tag{2}$$

Given the deformation gradient $\mathbf{F} \in R^{3\times 2}$ for a skin triangle, $I_1 = tr(\mathbf{F}^T\mathbf{F})$ and $J = \sqrt{det(\mathbf{F}^T\mathbf{F})}$ are the strain invariants used to evaluate the elastic energy. λ and μ are the Lamé parameters, α and β are material constants related to stiffening, and $k = 1 + \frac{\mu + \alpha\cdot\beta}{\lambda}$.

In the next paragraphs, we will extend this model to incorporate skin anisotropy, pre-stretch, and spatially varying adhesion. We will describe the following skin material model:

$$W_{Skin} = W_{Fung} + W_{Fiber} + W_{Ligament} \tag{3}$$

Collagen Fibers and Anisotropy. Collagen fibers induce anisotropic behavior in skin. From a computational perspective, these fibers lead to a higher stiffness of the material along their direction $\mathbf{d}$. To model this effect, we introduce the following term

$$W_{\text{Fiber}} = s^2, \quad s = \mathbf{d}^T\mathbf{F}^T\mathbf{F}\mathbf{d} - 1 \tag{4}$$

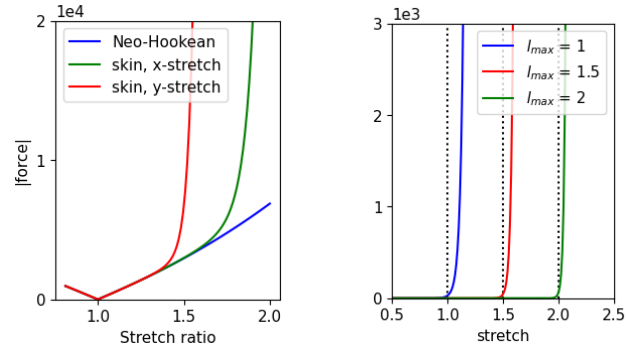

(a) Mterial models. (b) Ligaments response.

Figure 3. (a) Polynomial models, such as the Neo-Hookean, cannot represent skin stiffening and anisotropy. (b) Forces exerted by skin ligaments increase quickly when a sliding threshold l_{max} is exceeded. The range of motion for sliding is controlled by l_{max}.

where s^2 is the squared stretch along the fiber direction and $\mathbf{F}$ is the deformation gradient of the skin triangle. While fibers strongly resist stretching, they offer little resistance to compression, and instead they bend or buckle. We model this effect using a cubic filter $E_{\text{Fiber}}^{\text{filtered}}(s) = \max(0, s^3)$, which switches off resistance to compression in a C^2-continuous way. We combine these two regimes into a fiber energy term

$$W_{\text{Fiber}} = E_{\text{Fiber}}^{\text{filtered}}(s) \cdot (k_1 + k_2 \cdot e^{k_3 \cdot s}) \quad k_1, k_2, k_3 \in R \tag{5}$$

Collagen fibers create the stiffening effect along their direction and correlate with the Langer lines [35]. We therefore set the fiber direction $\mathbf{d}$ for each triangle element according to the local orientation of the Langer lines. Next, we explain how to determine the distribution of these lines along the body.

Langer Lines. Although Langer lines were already discovered in 1861 [21], they are still described through handmade drawings (as those shown in Figure 4). To the best of our knowledge, there exists no digital representation for Langer lines yet. To develop such a representation, we model Langer lines as continuous vector fields defined across arbitrary body shapes. We first define a sparse vector field on the body mesh by selecting a set of sample triangles and manually assigning the closest directions from the two-dimensional drawings. For each remaining triangle, we then find the closest sample and propagate its direction using parallel transport [15]. Since the resulting field is discontinuous, we apply an additional smoothing step. As can be seen in Figure 4, this algorithm produces smooth vector fields that closely resemble the input drawings.

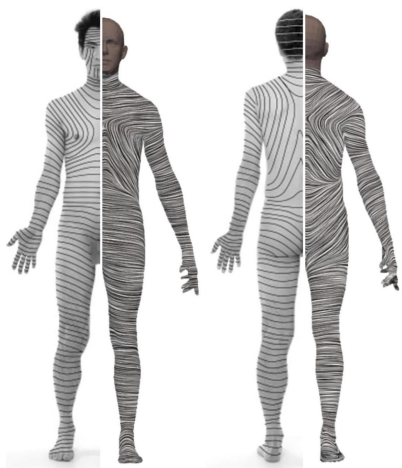

Figure 4. Langer lines. Split-view comparison of two-dimensional drawings (*left halves*) [30] and our continuous vector fields visualized using line integral convolution (*right halves*).

4.3. Modeling Pre-Stretch along Tension Lines

The significance of Langer lines for skin mechanics is widely recognized [35]. Nevertheless, we know of no computational model that would use Langer lines to model spatially varying pre-stretch across the body. To fill this gap, we leverage the continuous vector field representation described above to define per-triangle pre-stretch directions. We then impose a scalar pre-stretch α based on these directions. We incorporate pre-stretch using an approach similar to multiplicative plasticity and elastic growth theories [11]. To this end, we consider the deformation gradient $\mathbf{F}_{\text{geometry}}$ that provides a linear map from a given undeformed triangle element to its deformed configuration. To incorporate pre-stretch, we factorize the deformation gradient as

$$\mathbf{F}_{\text{geometry}} = \mathbf{F}_{\text{elastic}} \cdot \mathbf{F}_{\text{prestretch}}(\alpha, \mathbf{d}) \,, \tag{6}$$

where $\mathbf{F}_{\text{prestretch}} = \alpha \mathbf{d}\mathbf{d}^T$ is a pre-stretch deformation gradient. The elastic part of the deformation is described by $\mathbf{F}_{\text{elastic}}$. It is worth noting that evaluating the elastic energy and its derivatives requires the elastic deformation gradient, which is computed as

$$\mathbf{F}_{\text{elastic}} = \mathbf{F}_{\text{geometry}} \cdot \mathbf{F}_{\text{prestretch}}^{-1} \,. \tag{7}$$

Optimization-based Pre-Stretch Computation. Evaluating the deformation gradient for a given triangle requires a rest shape for the element. However, this rest shape is generally not known since (1) we do not have an explicit parameterization of the body mesh and (2) there exists no neutral pose in which all elements would be undeformed. For this reason, we aim to automatically compute optimal per-triangle rest shapes. Therefore, we seek to find rest shapes that minimize deformation across a set of example poses extracted from real-world motion capture data. For each triangle, let $\mathbf{F}_{ij} \in R^{3\times 2}$ denote the deformation gradient of triangle i for example pose j, i.e.,

$$\mathbf{F}_{ij} = \begin{bmatrix}\mathbf{e}_1 & \mathbf{e}_2\end{bmatrix} \begin{bmatrix}\bar{\mathbf{e}}_1 & \bar{\mathbf{e}}_2\end{bmatrix}^{-1} = E \cdot \bar{E}^{-1} \tag{8}$$

where $(\mathbf{e}_1, \mathbf{e}_2) \in R^{3\times 2}$ are the two edge vectors in the deformed configuration and $(\bar{\mathbf{e}}_1, \bar{\mathbf{e}}_2) \in R^{2\times 2}$ are the corresponding rest vectors in local triangle coordinates. The rest shape of the triangle is defined by three independent variables, corresponding to three 2D vertex positions $\{(0,0), (a_i, 0), (b_i, c_i)\}$, hence $\bar{E}^{-1}$ has coefficients $(h_i, k_i, 0, m_i)$. We obtain these values by solving the optimization problem

$$(\hat{\mathbf{h}}, \hat{\mathbf{k}}, \hat{\mathbf{m}}) = \text{argmin}_{(\mathbf{h},\mathbf{k},\mathbf{m})} \sum_{j}^{M} \sum_{i}^{N} ||\mathbf{F}_{ij}^T \mathbf{F}_{ij} - \mathbf{I}_2||^2 \,, \tag{9}$$

where $(\mathbf{h}, \mathbf{k}, \mathbf{m})$ are vectors holding the rest shape parameters for the N skin triangles. Visually, the above optimization problem minimizes a simple deformation measure across the entire set of P target poses. In our experiments, given a motion sequence of K frames, we sample $M = K/10$ evenly-spaced poses and solve the problem using Newton's method. The resulting per element rest poses are then used for computing deformation gradients when evaluation the skin energy and its derivatives.

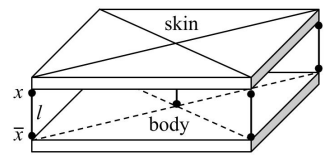

Figure 5. Skin, body, and ligaments. Illustration of ligament location $\mathbf{x}$, attachment point $\bar{\mathbf{x}}$, and length l.

4.4. Skin Ligaments

Skin ligaments are linear structures that connect the superficial layers of the skin to deep fascia, muscles, and bones. They bind the skin to soft and hard tissues, with an adhesion strength that depends on their lengths and density. Since these ligaments are not tensioned and run orthogonal to the skin's surface, they do not resist skin sliding to the first order. They are nevertheless firmly anchored and, once straightened, strongly oppose further sliding of the skin.

To capture these effects, we model skin ligaments as springs with an exponential material behavior. The rest length of the spring represents the distance at which the ligament is fully extended and exerts its response. The deformed length is: $l = ||\mathbf{x} - \tilde{\mathbf{x}}||_2$, where $\tilde{\mathbf{x}}$ and $\mathbf{x}$ are the rest and deformed locations of the ligament attachment points respectively (Fig. 5). We model the resistance of ligaments

as

$$W_{\text{Ligament}} = m_1 \cdot l^2 + m_2 \cdot \{e^{m_3 \cdot (l^2 - l_{\max}^2)}\}\,, \qquad (10)$$

where m_1, m_2, m_3 are material constants and $l_{\max}$ is the length at which the ligament is fully extended. The quadratic excursion $l^2 - l_{\max}^2$ causes a rapid stiffening when $l > l_{\max}$ and a soft compression response for $l < l_{\max}$.

5. Results

We evaluate our method on set of examples that compare skin deformations to baselines and experimental data.

5.1. Texture Sliding

To illustrate the impact of our method in a visually intuitive way, we investigate the skin deformations induced in the neck region when lifting the head. We constrain the skin at the boundary and place zero-length ligaments on the eyes, lips, nose, and ears to mimic the real-world behavior of skin in these areas. We employ a Young modulus of 3015, Poisson ratio of 0.33, $\alpha = 0.34$, $\beta = 6.62$, $k_1 = 0$, $k_2 = 0.002$, $k_3 = 7.9$, $m_1 = 0$, $m_2 = 0.0025$, and $m_3 = 7$. These parameters are the result of fitting our anisotropic material model on the measurements of [23, 24] for rabbit skin. We optimize the profile of the energy curve to guarantee consistent behavior along the directions parallel and orthogonal to the Langer lines. Triangle inversions in the simulation are prevented by detecting primitives collapsing to zero-area states during Newton iterations. In such case, the update is rejected, and the magnitude of the step is reduced. We visualize deformations using texture mapping. As can be seen in Fig. 6, the default SMPL skinning method leads to visible texture distortions below the chin, whereas our simulation-based method produces smooth deformations.

5.2. Langer Lines

Fig. 7 shows visualizations of our on-surface vector field representation of Langer lines. Our different body shapes share the same mesh topology, and the tension lines for arbitrary body shapes of the same gender are obtained using the same input sparse vector field. We use two different input fields for female and male body avatars as their tension lines differ in the torso region. Additional Langer lines for Dyna and SMPL avatars are illustrated in Fig. 1. We use aitviewer [14] to create the T-poses for the characters.

5.3. Motion Sequences on SMPL

We additionally evaluate skin deformations using real-world motion sequences. Skin ligaments are placed according to [34], with shorter lengths on areas with limited sliding (the popliteal fossae, cubital fossae, hands, wrists, feet, head, and the axilla) and no skin sliding (the belly button, the papilla mammae, and between the glutes). To obtain

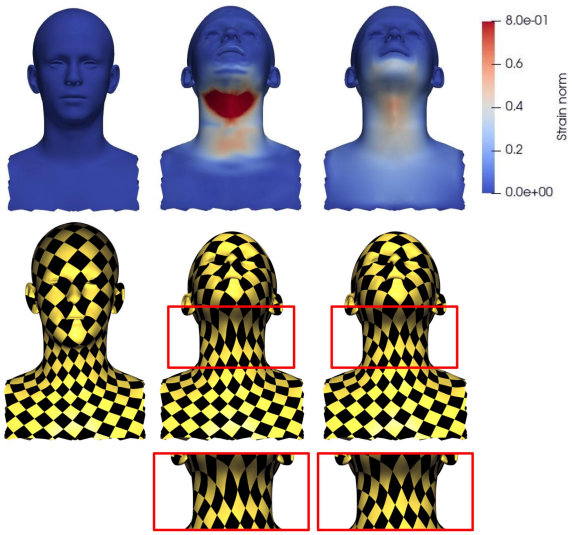

Figure 6. Skin simulation on head and neck. Comparison of deformations using color coding (*top*) and texturing (*bottom*) for SMPL's default skinning (*middle*) and our method (*right*).

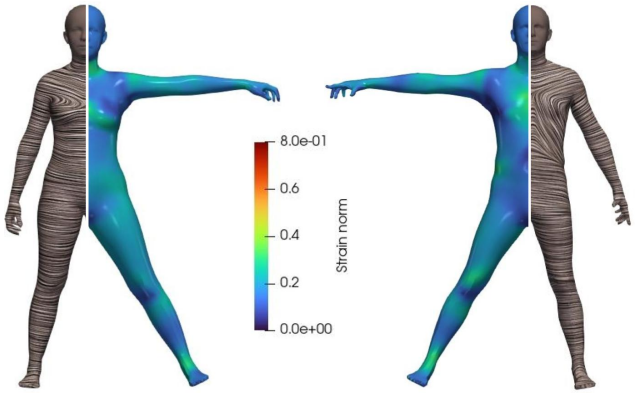

Figure 7. Langer lines and pre-stretch. Our method generalizes to different genders and body shapes. We also show the strain norm resulting from pre-stretch in the T-pose.

smoothly varying ligament lengths, we average values over one-ring neighborhoods. We use the rest shape optimization (Sec. 4.3) and apply a pre-stretch of 0.875 to every triangle element except for the head region (there, we apply a neutral color in the visualizations with color-coding). For the first frame of the sequences, we repeat the simulation adding exponential behavior, anisotropy, and pre-stretch in sequence. If the body displacement between two frames is large, we first simulate without the exponential terms.

Fig. 8 compares the skin deformation using SMPL's default skinning with our simulation results on two motion sequences from the AMASS datasets [28], MoSh and ACCAD. For SMPL's default skinning, the skin deformation exhibits visible noise and strain concentrations between

Figure 8. Dynamic motion sequences. We compare skin deformations for SMPL's default skinning (*bottom*) with our simulation-based method (*top*). On the left, we show the ligament lengths defined on the character body.

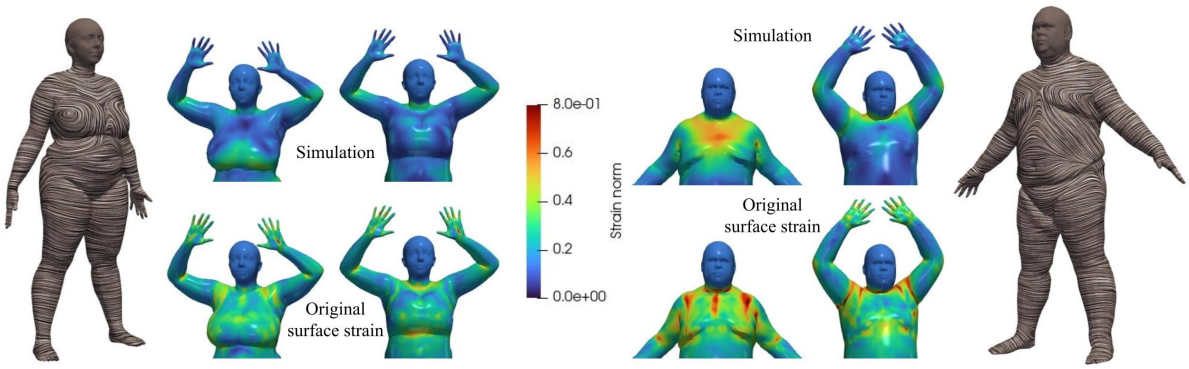

Figure 9. Our method applied to a Dyna dataset model with high BMI. We visualize Langer lines (*left*) and skin deformations using our simulation (*top*) and the original surface (*bottom*) on two avatars from the Dyna dataset.

thighs, shoulders, and legs. In contrast, our simulation-based method leads to a smooth distribution of deformations. We illustrate skin deformations on additional poses from the DanceDB and SSM datasets in Fig. 1.

In our experiments, we employed smoothness as a qualitative measure for validation. In fact, as a visco-elastic material, skin tends to exhibit spatially smooth deformations. In contrast, digital body models such as SMPL and Dyna exhibit noisy strain distributions with isolated peaks, which are biomechanically implausible.

5.4. Motion Sequences on Dyna

Apart from SMPL, we also applied ViSkin to two models from the Dyna dataset with high BMI, as they are optimized to have more realistic deformations. Fig. 9 shows a comparison between deformations on the original surface (bottom) and after simulation(top). We observe unnaturally noisy skin deformations on the original Dyna's surfaces, whereas our method produces smooth and plausible skin deformations.

5.5. Runtime

Table 1 shows the mean run-time to simulate a frame in the dynamic motion sequences presented above. We observe that a greater amount of time is required for pairs sequence-avatar with larger deformations. The timings are recorded on an i5-10300H CPU of 2.50GHz.

5.6. Skin Sliding on Palm and Wrist

We evaluate the effect of ligaments on skin sliding in the forearm region. We record the downward motion of the skin in the forearm region caused by pushing a skintight velcro band. Markers are drawn on the user's arm to better evaluate skin sliding. In digital space, we apply a realistic skin texture, and we color in black the constrained area of skin that slides downwards, mimicking the velcro band of our experimental setup. We place zero-length skin ligaments over the palm and 2cm long ligaments on the wrist and the cubital

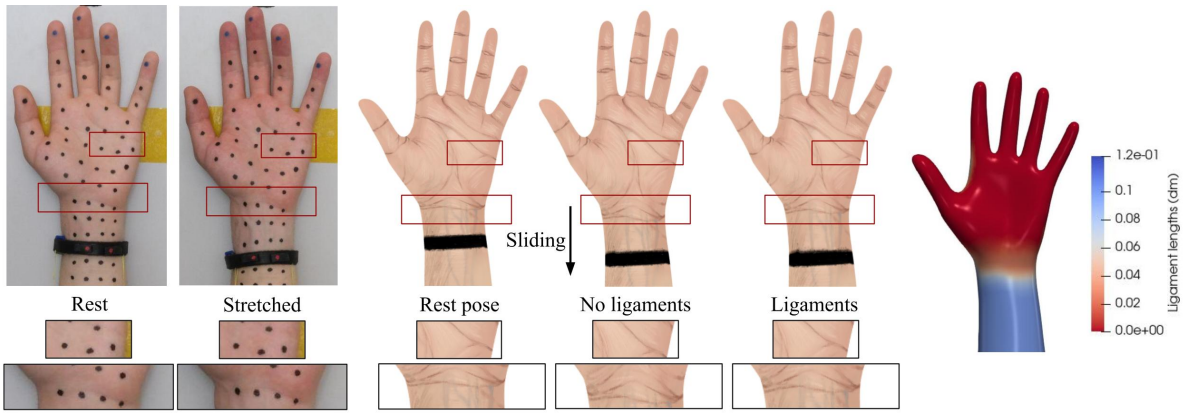

Figure 10. Skin sliding on palm and wrist. From *left* to *right*: Experimental capture of skin sliding (*1-2*) and comparison of simulation results without (4) and with (5) ligaments. The ligament lengths are shown to the far right.

Sequence Name	dataset	Mean Step Time
dance	SMPL, MoSH	0.6 *s*
kick	SMPL, ACCAD	0.25 *s*
dance	SMPL, SSM	13 *s*
dance	SMPL, DanceDB	0.9 *s*
jiggle on toes	Dyna	17 *s*
jumping jacks	Dyna	38 *s*

Table 1. Benchmarks on different motion sequences. Dynamic sequence with larger deformations take more computation time.

fossa. This value corresponds to the empirically determined maximum sliding lengths observed on the subject's arm. In Fig. 10, we show that without ligaments, the skin deforms unnaturally, similar to a glove sliding off the arm. When ligaments are used, the skin remains in place on the palm and deforms moderately on the wrist, which qualitatively agrees with our experimental observations.

We observe that the forearm is an ideal place to test skin stretching and sliding, as our experiments aim at isolating these effects from other factors to minimize confounding influences. To build intuition for this experiment, we invite readers to do a simple self-test: holding the right forearm below the wrist with the left hand (or vice versa), and pull the skin towards the elbow. Observe how skin motion extends well beyond knuckles with large sliding at the wrist and some stretching. The non-linearity of the skin can be clearly felt as a hard stop when further motion of the hand becomes impossible.

6. Conclusions

We have presented an automated method for simulating biomechanically plausible skin deformations on digital body models. Our model incorporates the most important characteristics of human skin, i.e., nonlinear and anisotropic material behavior, spatially varying pre-stretch, and bi-phasic sliding resistance mediated by skin ligaments.

6.1. Limitations & Future Work

Skin pre-stretch and elasticity parameters depend on factors such as age and the amount of adipose tissue. Our method currently does not try to model these variations. Nevertheless, developing a data-driven model to capture these effects is an interesting direction for future work.

Our skin model is computationally efficient and avoids collision handling. While our approach purposefully avoids modeling wrinkles, augmenting digital humans with simulated wrinkles would further increase realism.

Our model is purely elastic, which is sufficient for many applications that rely on quasi-static states of deformation. For more dynamic settings, viscous material properties become important and should be modeled as well.

Finally, using an exponential model allows for more accurate modeling of the skin's stretch response, but also introduces challenges for simulation.

We believe that our skin model provides a first step toward designing personalized sportswear, orthoses, and rehabilitation devices. Integrating our simulation model with optimization-based design tools for these applications is an exciting direction for future work.

7. Acknowledgments

We are grateful to the anonymous reviewers for their valuable comments. This work was supported by the European Research Council (ERC) under the European Union's Horizon 2020 research and in novation program (grant agreement No. 866480), and the Swiss National Science Foundation through SNF project grant 200021_200644.

References

[1] Irene Albrecht, Jörg Haber, and Hans-Peter Seidel. Construction and animation of anatomically based human hand models. In *Proceedings of the 2003 ACM SIGGRAPH/Eurographics Symposium on Computer Animation*, page 98–109, Goslar, DEU, 2003. Eurographics Association.

[2] Oleg Alexander, Mike Rogers, William Lambeth, Matt Chiang, and Paul Debevec. The digital emily project: photoreal facial modeling and animation. In *Acm siggraph 2009 courses*, pages 1–15. 2009.

[3] Dicko Ali-Hamadi, Tiantian Liu, Benjamin Gilles, Ladislav Kavan, François Faure, Olivier Palombi, and Marie-Paule Cani. Anatomy transfer. *ACM Trans. Graph.*, 32(6), 2013.

[4] Dragomir Anguelov, Praveen Srinivasan, Daphne Koller, Sebastian Thrun, Jim Rodgers, and James Davis. Scape: shape completion and animation of people. In *ACM SIGGRAPH 2005 Papers*, pages 408–416. 2005.

[5] Thabo Beeler, Fabian Hahn, Derek Bradley, Bernd Bickel, Paul Beardsley, Craig Gotsman, Robert W Sumner, and Markus Gross. High-quality passive facial performance capture using anchor frames. In *ACM SIGGRAPH 2011 papers*, pages 1–10. 2011.

[6] V Blanz and T Vetter. A morphable model for the synthesis of 3d faces. In *26th Annual Conference on Computer Graphics and Interactive Techniques (SIGGRAPH 1999)*, pages 187–194. ACM Press, 1999.

[7] Peter Brenner and Ghazi Rayan. Dupuytren's disease. 2003.

[8] H. T. Cox. The cleavage lines of the skin. *BJS (British Journal of Surgery)*, 29(114):234–240, 1941.

[9] Ye Fan, Joshua Litven, David I. W. Levin, and Dinesh K. Pai. Eulerian-on-lagrangian simulation. *ACM Trans. Graph.*, 32 (3), 2013.

[10] Y.C. Fung. *Biomechanics: Mechanical Properties of Living Tissues*. Springer New York, 1981.

[11] Alain Goriely, Mark Robertson-Tessi, Michael Tabor, and Rebecca Vandiver. *Elastic Growth Models*, pages 1–44. Springer Berlin Heidelberg, Berlin, Heidelberg, 2008.

[12] Rachel B. Groves, Sion A. Coulman, James C. Birchall, and Sam L. Evans. An anisotropic, hyperelastic model for skin: Experimental measurements, finite element modelling and identification of parameters for human and murine skin. *Journal of the Mechanical Behavior of Biomedical Materials*, 18:167–180, 2013.

[13] Hengtao Guo, Benjamin Planche, Meng Zheng, Srikrishna Karanam, Terrence Chen, and Ziyan Wu. Smpl-a: Modeling person-specific deformable anatomy. In *2022 IEEE/CVF Conference on Computer Vision and Pattern Recognition (CVPR)*, pages 20782–20791, 2022.

[14] Manuel Kaufmann, Velko Vechev, and Dario Mylonopoulos. aitviewer, 2022.

[15] Mathieu Desbrun Keenan Crane, Fernando de Goes and Peter Schröder. Digital geometry processing with discrete exterior calculus. In *ACM SIGGRAPH 2013 courses*, New York, NY, USA, 2013. ACM.

[16] Marilyn Keller, Silvia Zuffi, Michael J. Black, and Sergi Pujades. OSSO: Obtaining skeletal shape from outside. In *Proceedings IEEE/CVF Conf. on Computer Vision and Pattern Recognition (CVPR)*, pages 20492–20501, 2022.

[17] Marilyn Keller, Keenon Werling, Soyong Shin, Scott Delp, Sergi Pujades, Liu C. Karen, and Michael J. Black. From skin to skeleton: Towards biomechanically accurate 3d digital humans. In *ACM ToG, Proc. SIGGRAPH Asia*, 2023.

[18] Meekyoung Kim, Gerard Pons-Moll, Sergi Pujades, Seungbae Bang, Jinwook Kim, Michael J. Black, and Sung-Hee Lee. Data-driven physics for human soft tissue animation. *ACM Trans. Graph.*, 36(4), 2017.

[19] Theodore Kim, Fernando De Goes, and Hayley Iben. Anisotropic elasticity for inversion-safety and element rehabilitation. *ACM Trans. Graph.*, 38(4), 2019.

[20] Martin Komaritzan, Stephan Wenninger, and Mario Botsch. Inside humans: Creating a simple layered anatomical model from human surface scans. *Frontiers in Virtual Reality*, 2: 694244, 2021.

[21] Karl Langer. Zur anatomie und physilogie der haut. *Sitzungsbericht der mathematisch-naturwissenschaftlichen Classe der Kaiserlichen Academie der Wissenschaften*, 44:19–48, 1861.

[22] Klaus Langer. On the anatomy and physiology of the skin: I. the cleavability of the cutis. *British Journal of Plastic Surgery*, 31:3–8, 1978.

[23] Y Lanir and Y.C. Fung. Two-dimensional mechanical properties of rabbit skin—ii. experimental results. *Journal of Biomechanics*, 7(2):171–182, 1974.

[24] Y. Lanir and Y.C. Fung. Two-dimensional mechanical properties of rabbit skin—i. experimental system. *Journal of Biomechanics*, 7(1):29–34, 1974.

[25] R.J. Lapeer, P.D. Gasson, and V. Karri. Simulating plastic surgery: From human skin tensile tests, through hyperelastic finite element models to real-time haptics. *Progress in Biophysics and Molecular Biology*, 103(2):208–216, 2010. Special Issue on Biomechanical Modelling of Soft Tissue Motion.

[26] Duo Li, Shinjiro Sueda, Debanga R Neog, and Dinesh K Pai. Thin skin elastodynamics. *ACM Trans. Graph. (Proc. SIGGRAPH)*, 32(4):49:1–49:9, 2013.

[27] Matthew Loper, Naureen Mahmood, Javier Romero, Gerard Pons-Moll, and Michael J. Black. SMPL: A skinned multi-person linear model. *ACM Trans. Graphics (Proc. SIGGRAPH Asia)*, 34(6):248:1–248:16, 2015.

[28] Naureen Mahmood, Nima Ghorbani, Nikolaus F. Troje, Gerard Pons-Moll, and Michael J. Black. AMASS: Archive of motion capture as surface shapes. In *International Conference on Computer Vision*, pages 5442–5451, 2019.

[29] Aleka McAdams, Yongning Zhu, Andrew Selle, Mark Empey, Rasmus Tamstorf, Joseph Teran, and Eftychios Sifakis. Efficient elasticity for character skinning with contact and collisions. In *ACM SIGGRAPH 2011 Papers*, New York, NY, USA, 2011. Association for Computing Machinery.

[30] Marc André Meyers and Po-Yu Chen. Biological materials science: Biological materials, bioinspired materials, and biomaterials. *MRS Bulletin*, 40(7):612–613, 2015.

[31] V. Modi, L. Fulton, A. Jacobson, S. Sueda, and D.I.W. Levin. Emu: Efficient muscle simulation in deformation space. *Computer Graphics Forum*, 2020.

[32] Juan Montes, Bernhard Thomaszewski, Sudhir Mudur, and Tiberiu Popa. Computational design of skintight clothing. *ACM Trans. Graph.*, 39(4), 2020.

[33] Akihiko Murai, Q Youn Hong, Katsu Yamane, and Jessica Hodgins. Dynamic skin deformation simulation using musculoskeletal model and soft tissue dynamics. *Computational Visual Media*, 3, 2016.

[34] LG. Nash, MN. Phillips, H. Nicholson, R. Barnett, and M. Zhang. Skin ligaments: regional distribution and variation in morphology. *Clin Anat.*, 2004.

[35] Aisling Ní Annaidh, Karine Bruyère, Michel Destrade, Michael D. Gilchrist, and Mélanie Otténio. Characterization of the anisotropic mechanical properties of excised human skin. *Journal of the Mechanical Behavior of Biomedical Materials*, 5(1):139–148, 2012.

[36] Ahmed A A Osman, Timo Bolkart, and Michael J. Black. STAR: A sparse trained articulated human body regressor. In *European Conference on Computer Vision (ECCV)*, pages 598–613, 2020.

[37] Andrei Pissarenko and Marc A. Meyers. The materials science of skin: Analysis, characterization, and modeling. *Progress in Materials Science*, 110:100634, 2020.

[38] Gerard Pons-Moll, Javier Romero, Naureen Mahmood, and Michael J. Black. Dyna: A model of dynamic human shape in motion. *ACM Transactions on Graphics, (Proc. SIGGRAPH)*, 34(4):120:1–120:14, 2015.

[39] Pablo Ramón, Cristian Romero, Javier Tapia, and Miguel A. Otaduy. Sflsh: Shape-dependent soft-flesh avatars. In *SIGGRAPH Asia 2023 Conference Papers*, New York, NY, USA, 2023. Association for Computing Machinery.

[40] Cristian Romero, Miguel Otaduy, Dan Casas, and Jesus Perez. Modeling and estimation of nonlinear skin mechanics for animated avatars. *Computer Graphics Forum*, 39:77–88, 2020.

[41] Igor Santesteban, Elena Garces, Miguel A. Otaduy, and Dan Casas. SoftSMPL: Data-driven Modeling of Nonlinear Soft-tissue Dynamics for Parametric Humans. *Computer Graphics Forum (Proc. Eurographics)*, 2020.

[42] Karthik Shetty, Annette Birkhold, Srikrishna Jaganathan, Norbert Strobel, Bernhard Egger, Markus Kowarschik, and Andreas Maier. Boss: Bones, organs and skin shape model. *Computers in Biology and Medicine*, 165:107383, 2023.

[43] Breannan Smith, Fernando De Goes, and Theodore Kim. Stable neo-hookean flesh simulation. *ACM Trans. Graph.*, 37(2), 2018.

[44] C. Stecco, V. Macchi, A. Porzionato, F. Duparc, and R. De Caro. The fascia: the forgotten structure. *Italian journal of anatomy and embryology*, 2011.

[45] Shinjiro Sueda, Andrew Kaufman, and Dinesh K. Pai. Musculotendon simulation for hand animation. *ACM Trans. Graph. (Proc. SIGGRAPH)*, 27(3), 2008.

[46] Shinjiro Sueda, Garrett L. Jones, David I. W. Levin, and Dinesh K. Pai. Large-scale dynamic simulation of highly constrained strands. *ACM Trans. Graph.*, 30(4), 2011.

[47] J. Teran, S. Blemker, V. Ng Thow Hing, and R. Fedkiw. Finite volume methods for the simulation of skeletal muscle. In *Proceedings of the 2003 ACM SIGGRAPH/Eurographics Symposium on Computer Animation*, page 68–74, Goslar, DEU, 2003. Eurographics Association.

[48] Joseph Teran, Eftychios Sifakis, Geoffrey Irving, and Ronald Fedkiw. Robust quasistatic finite elements and flesh simulation. In *Proceedings of the 2005 ACM SIGGRAPH/Eurographics Symposium on Computer Animation*, page 181–190, New York, NY, USA, 2005. Association for Computing Machinery.

[49] Demetri Terzopoulos and Keith Waters. Physically-based facial modelling, analysis, and animation. *Comput. Animat. Virtual Worlds*, 1:73–80, 1990.

[50] Velko Vechev, Ronan Hinchet, Stelian Coros, Bernhard Thomaszewski, and Otmar Hilliges. Computational design of active kinesthetic garments. In *Proceedings of the 35th Annual ACM Symposium on User Interface Software and Technology*, New York, NY, USA, 2022. Association for Computing Machinery.

[51] Nicholas J. Weidner, Kyle Piddington, David I. W. Levin, and Shinjiro Sueda. Eulerian-on-lagrangian cloth simulation. *ACM Trans. Graph.*, 37(4), 2018.

[52] Jeffrey A. Weiss, Bradley N. Maker, and Sanjay Govindjee. Finite element implementation of incompressible, transversely isotropic hyperelasticity. *Computer Methods in Applied Mechanics and Engineering*, 135(1):107–128, 1996.

[53] Jane Wilhelms and Allen Van Gelder. Anatomically based modeling. In *Proceedings of the 24th Annual Conference on Computer Graphics and Interactive Techniques*, page 173–180, USA, 1997. ACM Press/Addison-Wesley Publishing Co.

[54] Yin Wu, Prem Kalra, and Nadia Magnenat Thalmann. Simulation of static and dynamic wrinkles of skin. In *Proceedings of the Computer Animation*, page 90, USA, 1996. IEEE Computer Society.